

1 Article

# 2 Greatly enhanced photovoltaic performance of 3 crystalline silicon solar cells using metal oxide layers 4 by band-gap alignment engineering

5 Lingling Zhou<sup>1</sup>, Lufei Xiao<sup>1</sup>, Hai Yang<sup>2</sup>, Jie Liu<sup>2,\*</sup> and Xibin Yu<sup>2,\*</sup>

6 <sup>1</sup>Department of Food and Environmental Engineering, Chuzhou Vocational and Technical College, Chuzhou  
7 239000, P. R. China. E-mail: zhoulingling2018@gmail.com (L.Z.); tangshiyong001@gmail.com (L.X.)

8 <sup>2</sup>The Education Ministry Key Laboratory of Resource Chemistry and Shanghai Key Laboratory of Rare Earth  
9 Functional Materials, Department of Chemistry, Shanghai Normal University, Shanghai 200234, P. R. China.  
10 E-mail: benjaejong@gmail.com (H.Y.)

11 \*Correspondence: E-mail: liujie@shnu.edu.cn (J.L.); xibinyu@shnu.edu.cn (X.Y.); Tel.: +86-21-64324528

12 **Abstract:** Band-gap alignment engineering has now been extensively studied due to its high  
13 potential application. Here we demonstrate a simple route to synthesize two metal oxide layers and  
14 align them together according to their bandgaps on surface of crystalline silicon (c-Si) solar cells.  
15 The metal oxide layers can not only extend absorption spectrum to generate extra carriers but also  
16 serve to separate electron-hole pairs more efficiently. As a consequence, the photovoltaic  
17 performance of SnO<sub>2</sub>/CdO /Si double-layer solar cell (DLSC) is highly improved compared to  
18 CdO/Si and SnO<sub>2</sub>/Si single-layer solar cells (SLSCs) and SnO<sub>2</sub>/CdO/Si double-layer solar cell  
19 (DLSC). By the alignment engineering, the SnO<sub>2</sub>/CdO/Si DLSC produces a short circuit  
20 photocurrent ( $J_{sc}$ ) of 38.20 mA/cm<sup>2</sup>, an open circuit photovoltage ( $V_{oc}$ ) of 0.575 V and a fill factor  
21 (FF) of 68.7%, corresponding to a light to electric power conversion efficiency ( $\eta$ ) of 15.09% under  
22 AM1.5 illumination. These results suggest that with the use of metal oxide layers by band-gap  
23 alignment engineering, new avenues have been opened for developing high-efficiency and  
24 cost-effective c-Si solar cells.

25 **Keywords:** silicon solar cells; semiconductors; electron-hole pairs

26

## 27 1. Introduction

28 Solar cells have now been developed for more than five decades. From the very first generation solar cell  
29 to the latest one, the conversion efficiency of solar cell itself has been largely improved. The update conversion  
30 efficiency of GaInP/GaAs solar cells have broken 40%<sup>1-4</sup>. However, these high efficiency solar cells still have  
31 many disadvantages, such as stability issue and high cost, so that they can hardly be put into large-scale  
32 production. At this point, with the combination of high purity, natural abundance, a matching insulator and  
33 maturity of production<sup>5,6</sup>, crystalline silicon (c-Si) solar cells show their unique advantageous properties. But  
34 still, there are several defects of c-Si solar cells, such as optical loss, recombination and thermal or quantum  
35 losses<sup>7</sup>. Among them, optical loss and recombination are deemed to be two most vital factors. Yet many efforts  
36 have been made by researchers to solve these problems. Silicon nanowires<sup>8-10</sup>, ZnO nanowires<sup>11</sup>, and CuO  
37 nanoleaves<sup>12</sup>, are some of those extraordinary attempts. The power conversion efficiency has been improved  
38 through light trapping enhancement and photocarrier collection facilitation<sup>13-14</sup>. It has opened up new  
39 opportunities to achieve higher energy conversion efficiency at lower fabrication costs.

40 Although many textured structures have been made to enhance absorptance of c-Si solar cells, c-Si is still  
41 an indirect band-gap semiconductor with a bandgap of 1.12eV, which is able to utilize only a small fraction of  
42 the solar spectrum. Currently, tandem solar cell is considered to be one of the most promising approaches of the  
43 third generation solar cells to solve this problem. It is fabricated with more than one sub cells which are  
44 tandemed according to their bandgaps<sup>15-16</sup>. It is reported that the overall open circuit voltage ( $V_{oc}$ ) is the sum of  
45 those from all individual sub-cells, while the current is the same as that in a single sub-cell once their currents

46 are matched<sup>17-19</sup>. As a result, tandem solar cell has broadened absorption spectrum effectively, so that it can  
47 tackle simultaneously absorption and thermalization losses by absorbing the higher energy photons and finally  
48 improve conversion performance.

49 By using the concept of tandem solar cells for reference, band-gap alignment engineering has been  
50 developed for various applications, such as quantum dot solar cells through band alignment engineering<sup>20</sup>.  
51 Here we applied CdO and SnO<sub>2</sub> semiconductors to c-Si solar cells. CdO is one of the transparent conducting  
52 oxides(TCOs) that has both, moderate band-gap and high electrical conductivity. With high mobility, CdO is  
53 also believed to have large potential for the use in active electronic devices<sup>21-22</sup>. SnO<sub>2</sub> nanostructures are always  
54 applied to gas sensor and photocatalysis<sup>23</sup>. Besides, with wide bandgap of 3.5~4.0eV and terrific electronic  
55 conductivity, it is believed to have a great prospect in solar cells. Herein, in our research we have tried to  
56 synthesize different nano-structured films of CdO and SnO<sub>2</sub> semiconductors on surface of c-Si substrate  
57 respectively. To investigate electrical properties and photovoltaic performance, we compared as-synthesized  
58 solar cells with CdO single layer to cells with SnO<sub>2</sub> single layer and cells with CdO layer and SnO<sub>2</sub> layer stacked  
59 together in the order of their bandgaps. CdO/Si single-layer solar cell (SLSC) and SnO<sub>2</sub>/Si single layer solar cell  
60 were produced with chemical bath deposition and spin-coating method after which a certain temperature  
61 thermal treatment was conducted to form oxide layers. Two steps of thermal treatment were included in  
62 synthesis of SnO<sub>2</sub>/CdO/Si double-layer solar cell (DLSC) to confirm a firm contact between double layers and  
63 the Si substrate. It is found that the characteristics of SnO<sub>2</sub>/CdO/Si DLSC offer broad-band light harvesting and  
64 super high minority carrier lifetime. Here we compare two SLSCs to SnO<sub>2</sub>/CdO/Si DLSC to demonstrate the  
65 impact of different layers with different bandgaps on absorption region and charge-transfer efficiency. As a  
66 result, the short-circuit current ( $J_{sc}$ ) and the open circuit voltage were improved which led to the enhancement  
67 of power conversion efficiency (PCE). We believe that the cost effective technology can be easily applied to the  
68 industrial scale production of Si solar cells.

## 69 2. Materials and Methods

### 70 Synthetic procedures

71 Slices (3.0×3.0 cm<sup>2</sup>) of c-Si wafers without Si<sub>3</sub>N<sub>4</sub> antireflection layer were applied in this work. The  
72 thickness of wafers is ~200μm with a bulk *p-n* junction. Before growing any film on the surface of Si  
73 wafer was first cleaned by rinsing with double distilled water and ethanol to eliminate any impurities.  
74 Firstly, two depositing solutions were prepared as solution A and B. Solution A was composed by  
75 0.05M Cadmium acetate dihydrate [Cd(CH<sub>3</sub>COO)<sub>2</sub>·H<sub>2</sub>O] and double distilled water. In solution B,  
76 0.01M Stannic chloride pentahydrate aqueous was mixed with ethanol to prohibit the solution from  
77 hydrolyzing. In order to grow CdO single layer on surface of Si wafers, dried Si wafer was immersed in  
78 solution A for 2mins and was dried again in drying oven under the temperature of 80°C. This  
79 procedure then was repeated for four more times to ensure the CdO seeds were fully distributed on the  
80 silicon's surface before sending the deposited Si wafer into muffle furnace. After thermal treatment of  
81 500°C for 3 mins, the CdO/Si SLSC was completed. SnO<sub>2</sub>/Si SLSC was synthesized by spin-coating  
82 method. In this step, firstly, 0.05 mL of 0.01M Stannic chloride pentahydrate aqueous ethanol solution  
83 were dropped onto Si surface under the speed of 1500 rpm for 40s, and 5 times of this operation were  
84 needed to ensure the Sn-precursor got the substrate full covered. Finally the deposited Si wafer was  
85 treated under 900°C in muffle furnace for 5 mins to form SnO<sub>2</sub> film. With combination of two  
86 procedures above, SnO<sub>2</sub> seed solution was deposited on surface of as-synthesized CdO/Si composited  
87 cell and 900°C annealing treatment was also conducted.

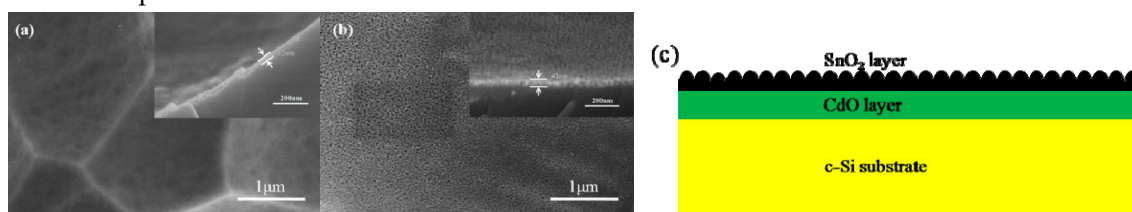
### 88 Characterization

89 Field emission scanning electron microscopic (FESEM, HitachiS-4800) was used to observe the  
90 morphology of the layers. The minority carrier lifetime of the samples are measured using the Si wafer  
91 life-time SEMILAB WT-2000 PVN. The current density-voltage (*J-V*) characteristics of the solar cells  
92 are measured using an electrochemical workstation (Zahner, Zennium) under 100 mW×cm<sup>-2</sup>  
93 calibration which is performed using a Class A AM 1.5G spectral distributed Abet Technologies Sun  
94 2000 Solar Simulator.

95  
96  
97

### 98 3. Results and discussion

99 Fig. 1 shows the surface morphologies of both CdO and SnO<sub>2</sub> films growing on the surface of  
 100 polycrystalline silicon with p-n junction respectively. As shown in Fig. 1 (a), CdO film was  
 101 characterized by Scanning Electron Microscope (SEM). The cross-section view indicates that the  
 102 thickness of the film is about 32nm, and the surface of it is smooth with comparison of top view  
 103 picture. While in Figure 1 (b), SnO<sub>2</sub> film shows a different surface morphology with many hollows  
 104 on it, and it is approximately 41nm in thickness which is slightly thicker than CdO film. With those  
 105 pictures we can find that both of two films have a firm contact with Si substrates, which is beneficial  
 106 to reduce contact resistance and electron transfer. Fig. 1(c) demonstrates the schematic of  
 107 SnO<sub>2</sub>/CdO/Si DLSC. With spin-coating method and annealing treatments, CdO layer and SnO<sub>2</sub> layer  
 108 were grown on Si substrate in sequence. On one hand, the top layer with rough surface of SnO<sub>2</sub> can  
 109 efficiently increase light trapping. On the other hand, two layers are capable to utilize different  
 110 region of incident light which is believed to contributed to considerable enhancement of  
 111 photovoltaic performance.



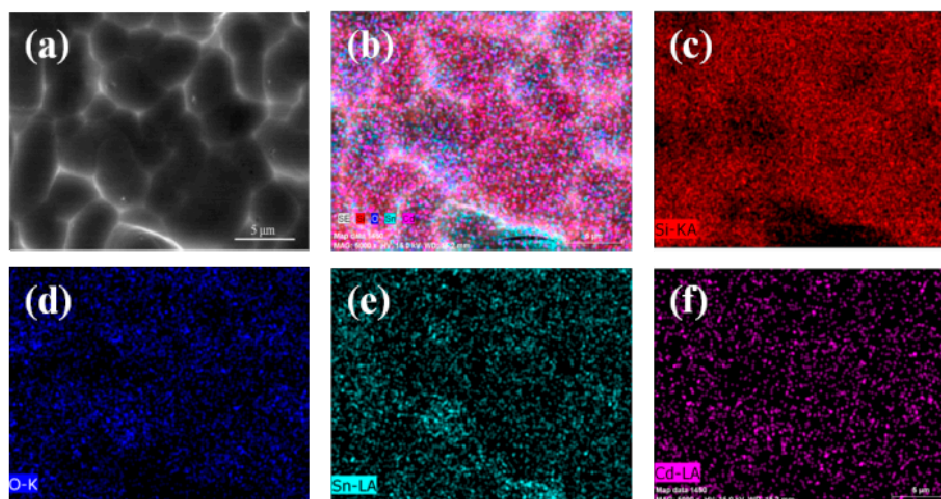
112

113 **Figure 1.** Cross-section and top views of SEM morphologies of (a) CdO; and (b) SnO<sub>2</sub>films growing on  
 114 polycrystalline silicon substrates respectively; (c) Schematic of SnO<sub>2</sub>/CdO/Si DLSC.

115 FESEM energy dispersive spectrometry (EDS) element mapping of composited SnO<sub>2</sub>/CdO/Si  
 116 DLSC was conducted to take deep research on the structure of layer-by-layer. As we can see in Fig. 2,  
 117 (a) is the scanning region of SnO<sub>2</sub>/CdO/Si composited wafer, while Fig 2 (b) is mapping of all  
 118 detected elements. Fig. 2 (c)~Fig. 2 (f) refer to element Si, O, Sn and Cd respectively. From Fig. 2 (c) to  
 119 Fig. 2 (f) we can find that the elements are well-distributed on the surface of c-Si substrate which  
 120 indicates that the layer-by-layer structure was greatly formed by spin-coating and annealing  
 121 procedures.

122

123



124

125

Figure 2. FESEM-EDS element mapping of the composited SnO<sub>2</sub>/CdO/Si DLSC.

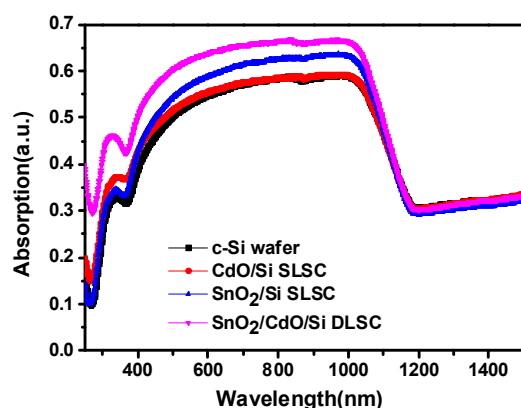
126

127

128

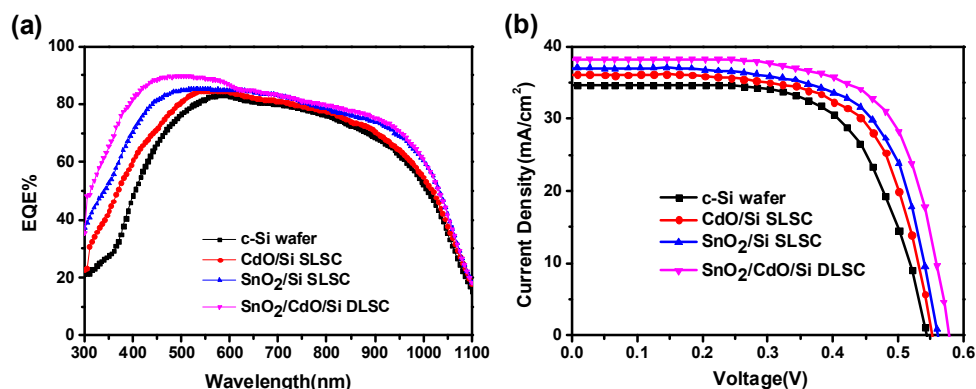
According to different morphologies above, different absorption spectra were measured by  
 UV-vis-IR. In Fig. 3, Si substrate with CdO layer shows almost the same absorption property as Si  
 wafer except the slight improvement between 300-450nm. But as to SnO<sub>2</sub> layer, from 300-1100 nm  
 the absorption value is improved by about 16%. The reason contributed to this phenomenon is that  
 the difference of surface structures. With hollows on surface, the film can cause optical resonance

129 and multiple scattering of the incident light, which can trap incident light and enhance absorptance  
 130 effectively<sup>24-26</sup>. In addition, due to its wide bandgap SnO<sub>2</sub> film is capable to utilize much more light  
 131 compared to c-Si wafer.



132  
 133 **Figure 3.** UV-vis-IR absorption spectra for CdO/Si and SnO<sub>2</sub>/Si SLSCs and SnO<sub>2</sub>/CdO/Si DLSC.

134 To further investigate photovoltaic properties of composited solar cells, External Quantum  
 135 Efficiency (EQE) spectra and J-V curves were conducted under the standard AM 1.5G conditions. Fig.  
 136 4 (a) shows that a broad value of 70% ~ 80% in the spectrum of pristine Si solar cell is observed from  
 137 500~900nm which corresponds to the wavelength range of Si light absorption. In contrast, the  
 138 spectrum of SnO<sub>2</sub>/Si SLSC exhibits a large increase in EQE spectrum for the wavelength between  
 139 300~550nm, while CdO/Si SLSC is a little low than that of SnO<sub>2</sub>/Si SLSC. On one hand, as two  
 140 semiconductors with wide bandgap ( $E_{gCdO} = 2.4\text{eV}$ ,  $E_{gSnO_2} = 3.5\text{eV}$ ), CdO and SnO<sub>2</sub> can effectively  
 141 absorb spectrum wavelength between 250~600nm. That means the CdO layer and SnO<sub>2</sub> layer are  
 142 able to use incident light from 250~600nm and generate more carrier with high energy while c-Si can  
 143 not. On the other hand, according to UV-vis-IR absorption spectra, both CdO/Si SLSC and SnO<sub>2</sub>/Si  
 144 SLSC have been enhanced between 300~500nm. As we know, if solar cells absorb more incident light,  
 145 more photons can be utilized to generate carriers. So the improvement of EQE can be also attributed  
 146 to the enhancement of absorption performance. Finally, the EQE performance of SnO<sub>2</sub>/CdO/Si DLSC  
 147 matches the theory we discussed above as well.



148  
 149 **Figure 4.** (a) External Quantum Efficiency (EQE) spectra and (b) J-V characteristics for CdO/Si and SnO<sub>2</sub>/Si  
 150 SLSCs and SnO<sub>2</sub>/CdO/Si DLSC.

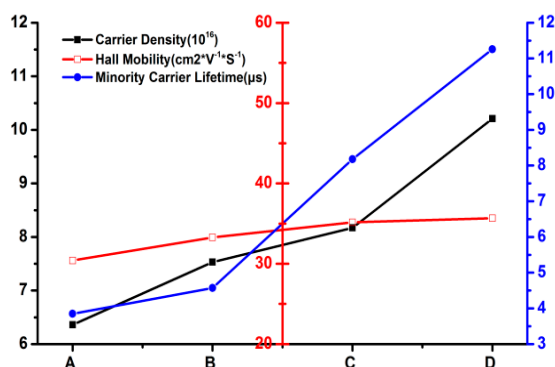
151 The detailed device performance is summarized in Table 1 and the J-V characteristic curves are  
 152 shown in Figure 4 (b). As a result, the PCE of CdO/Si SLSC reaches a value as high as 13.34%, with  $J_{sc}$   
 153 of 36.12 mA cm<sup>-2</sup>,  $V_{oc}$  of 0.556V and FF of 66.42%, while values of SnO<sub>2</sub>/Si SLSC are 13.96%, 37.01mA  
 154 cm<sup>-2</sup>, 66.76% respectively. Compared to pristine Si solar cell without any metal oxide film growing  
 155 on the top, the  $V_{oc}$  performance are improved by 2.6% and 4.2%. Whereas as to current density,  
 156 three as-synthesized solar cells all have various increases compared to blank Si solar cell. The

157 short-circuit current are mainly related with three factors as we concluded, and the very first one is  
 158 light absorption. The photoactive layer in the solar device absorbs sun light, raising an electron  
 159 from the ground state to a higher energy state and then generates an energy bearing electron-hole  
 160 pair, called an excitation<sup>27</sup>. As we know, c-Si is a indirect band-gap semi-conductor with a band-gap of  
 161 1.12eV and the perfect light spectra region for absorption of c-Si is approximately 700~1100 nm  
 162 which is only a small part of the whole solar spectrum. So to make full use of the solar spectrum in  
 163 order to maximize  $J_{sc}$ , light-absorbing substance is now fully used. As the more solar spectrum is  
 164 utilized, the more photo-generated carriers are produced. But a large part of these photo-generated  
 165 carriers are wasted directly through recombination. It indicates that if electron-hole pairs can be  
 166 efficiently separated before recombination,  $J_{sc}$  value is supposed to be enhanced to a large extend. In  
 167 addition, to ensure an efficient collection of charge carriers, carrier transporting layers are required  
 168 to have high mobility as well as long diffusion lengths for electrons and holes<sup>28-30</sup>, and the resistance  
 169 is also a factor that changes current flowing. In our research,  $J_{sc}$  of CdO/Si and SnO<sub>2</sub>/Si solar cells are  
 170 increased to 36.12mA cm<sup>-2</sup> and 37.01mA cm<sup>-2</sup>. The increasement can be ascribed to absorption  
 171 enhancement as shown in Fig. 3 (a) and charge carrier lifetime increase shown in Fig. 5.

172 **Table 1** Photovoltaic performance parameters of blank c-Si solar cell and as-synthesized CdO/Si  
 173 and SnO<sub>2</sub>/Si SLSCs and SnO<sub>2</sub>/CdO/Si DLSC.

|                          | V <sub>oc</sub> [V] | J <sub>sc</sub> [mA cm <sup>-2</sup> ] | FF[%] | η [%] | Δη[%] |
|--------------------------|---------------------|----------------------------------------|-------|-------|-------|
| c-Si                     | 0.542               | 34.68                                  | 65.33 | 12.28 | --    |
| CdO/Si                   | 0.556               | 36.12                                  | 66.42 | 13.34 | 8.6   |
| SnO <sub>2</sub> /Si     | 0.565               | 37.01                                  | 66.76 | 13.96 | 13.6  |
| SnO <sub>2</sub> /CdO/Si | 0.575               | 38.20                                  | 68.70 | 15.09 | 22.8  |

174



175

176 **Figure 5.** Carrier density, Hall mobility and minority carrier lifetime properties of A (c-Si solar cell ), B (CdO/Si  
 177 SLSC), C (SnO<sub>2</sub>/Si SLSC) and D (SnO<sub>2</sub>/CdO/Si DLSC ).

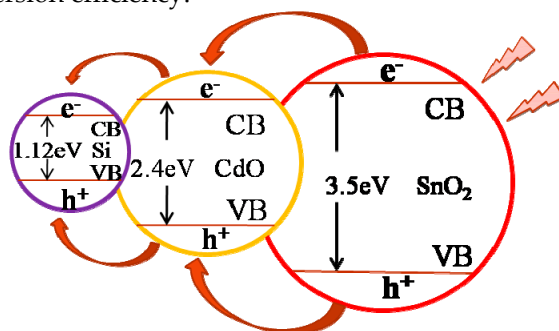
178 In Fig. 5 we can also find that carrier density values of three kinds of as-synthesized solar cells  
 179 are all enhanced. As we discussed above, because of good solar spectrum absorption property and  
 180 band-gap alignment engineering, the composited solar cells are able to make better use of solar  
 181 spectra and thus produce more photo-generated carriers. Carrier density is a important parameter to  
 182 measure the utilized efficiency of absorbed photons. For CdO owns a wider bandgap than c-Si,  
 183 spectrum region of short wavelength is fully used according to results of UV-vis-IR absorption and  
 184 EQE property shown in Fig. 3. For the same reason, as bandgap of SnO<sub>2</sub> is even wider, the EQE and  
 185 UV-vis-IR results indicate the enhancement of carrier density which is correspondence with that  
 186 measured in Fig. 5. Moreover, Hall mobility is highly related to electrical conductivity. The result in  
 187 Fig. 5 (red line) shows that with CdO layer and SnO<sub>2</sub> layer growing on top of c-Si substrates, the  
 188 speed of carrier transport is not decayed but improved instead. This phenomenon demonstrates that  
 189 CdO layer and SnO<sub>2</sub> layer we have synthesized play a role as good electron transport layers. When  
 190 CdO and SnO<sub>2</sub> were made to grow on surface of c-Si substrates by spin coating method,  
 191 homogeneous films were produced through tuning spinning speed and coating time. After

192 annealing at 500°C and 900°C orderly, thin oxide films then were formed with a firm Ohmic contact  
 193 with c-Si substrates which is supposed to decrease series resistance. Besides, blue line is put to  
 194 demonstrate the change of minority carrier lifetime., and the result shows that after covered by  
 195 different oxide layers, lifetime of minority carrier is highly increased. The effective carrier lifetime  
 196 ( $\tau_{\text{eff}}$ ) is directly related to bulk lifetime ( $\tau_{\text{bulk}}$ ) and surface lifetime ( $\tau_{\text{surf}}$ ) and the  $\tau_{\text{bulk}}$  dominates the  
 197  $\tau_{\text{eff}}$ <sup>31</sup>. The increase in JSC and VOC partly contributed by improved minority carrier lifetime can be  
 198 understood by the relations below<sup>32</sup>.

$$V_{oc} = \frac{kt}{q} \ln\left(\frac{\Delta n(N_{D,A} + \Delta n)}{n_i^2}\right) \quad (1)$$

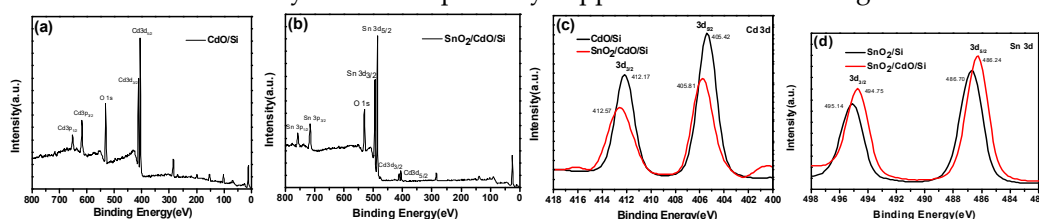
$$J_{sc} = qG(L_n + L_p) \quad (2)$$

201 where  $(kT)/q$  is the thermal voltage,  $N_{D,A}$  is the donor or acceptor concentration of the wafer,  
 202  $\Delta n$  is the excess carrier concentration,  $n_i$  is the intrinsic carrier concentration,  $q$  is the magnitude of  
 203 the electrical charge on the electron,  $G$  is the generation rate, and  $L_n$  and  $L_p$  are electron and hole  
 204 diffusion lengths, respectively. We can find that  $V_{oc}$  and  $J_{sc}$  strongly depend on excess carrier  
 205 concentration and diffusion lengths which are directly proportional to the  $\tau_{\text{eff}}$ . That is to say, the  
 206 increase of minority carrier lifetime gives rise to the enhancement of  $J_{sc}$  and  $V_{oc}$  and which in the end  
 207 contribute to power conversion efficiency.



208  
 209 **Scheme 1.** Schematic diagram representing the charge-transfer and electron-hole separation process in  
 210 SnO<sub>2</sub>/CdO/Si DLSC.

211 To further investigate the mechanism of charge-transfer and electron-hole separation, we here  
 212 illustrate the schematic diagram representing charge-transfer and electron-hole separation process  
 213 in Scheme 1. As shown in the diagram, the conduction band (CB) of SnO<sub>2</sub> lies at a more negative  
 214 potential than that of CdO, while the valence band (VB) of CdO is more negative than that of SnO<sub>2</sub>.  
 215 Under solar irradiation, photo-generated electrons in the conduction band of SnO<sub>2</sub> go to the  
 216 conduction band of CdO and hole transfer occurs from the valence band of CdO to that of SnO<sub>2</sub>. At  
 217 the same time, with a similar reason for c-Si substrate, electrons from conduction band of CdO  
 218 transfer to that of c-Si and holes transfer from valence band of CdO to that of c-Si. The simultaneous  
 219 transfer of electrons and holes in SnO<sub>2</sub>/CdO/Si system increase both the yield and the lifetime of  
 220 charge carriers by separating the photo-induced electrons and reducing charge recombination in  
 221 electron-transfer process<sup>33</sup>. In our research, the results of minority carrier lifetime, carrier density  
 222 and short current density are able to perfectly support the schematic diagram we discussed above.



223  
 224 **Fig. 6** XPS survey spectra of (a) CdO/Si SLSC and (b) composited SnO<sub>2</sub>/CdO/Si DLSC. Core level (c) Cd 3d, (d) Sn 3d XPS  
 225 spectra.

226 X-ray photoelectron spectroscopy (XPS) was also conducted to study the compositions and  
227 chemical states of as-synthesized SnO<sub>2</sub>/CdO/Si composited solar cell. Fig.6 (a), (b) compare the XPS  
228 survey spectrum of CdO/Si and SnO<sub>2</sub>/CdO/Si. In comparison to CdO/Si, the XPS survey spectrum of  
229 SnO<sub>2</sub>/CdO/Si exhibits four additional Sn peaks, and two strongest peaks refer to Sn 3d<sub>3/2</sub> and Sn 3d<sub>5/2</sub>.  
230 When focusing on Cd 3d, we can find that peaks of Cd 3d in Fig. 6 (b) are apparently much weaker  
231 than that in Figure 6 (a). Because of a ~40nm thickness SnO<sub>2</sub> layer covered on top of CdO layer with  
232 spin-coating method, XPS signal of Cd was heavily blocked by SnO<sub>2</sub> layer. The Cd 3d core level  
233 spectra of CdO/Si solar cell and SnO<sub>2</sub>/CdO/Si solar cell are shown in Fig. 6 (c). For CdO/Si, peaks of  
234 Cd 3d center at 405.42eV and 412.17eV which are consistent with the values reported for Cd<sup>2+</sup>, while  
235 peaks of Cd 3d<sub>5/2</sub> and Cd 3d<sub>3/2</sub> are located at 405.81eV and 412.57eV respectively for SnO<sub>2</sub>/CdO/Si  
236 solar cell<sup>34</sup>. There is about a 0.4eV increasement in binding energy of Cd 3d between CdO/Si and  
237 SnO<sub>2</sub>/CdO/Si, which illustrates that the extraction of nuclei and electrons becomes stronger. It is  
238 believed that SnO<sub>2</sub> crystalline and CdO crystalline are affected by each other and formed a kind of  
239 hetero-structure. This new formation of structure gives a vital impact on carrier-transport between  
240 different layers and also leads to a drastic improvement in the photovoltaic performance of  
241 SnO<sub>2</sub>/CdO/Si DLSC.

#### 242 4. Conclusions

243 In conclusion, we investigated the photovoltaic performance of crystalline silicon solar cells  
244 using different metal oxide layers by band-gap alignment engineering that act as wavelength  
245 broadening layers for optical absorption and effective carrier separation and transport layers. The  
246 photovoltaic performance of as-synthesized SnO<sub>2</sub>/Si SLSC, CdO/Si SLSC and SnO<sub>2</sub>/CdO/Si DLSC  
247 were considerably improved in comparison with original c-Si solar cells. The highest PCE value  
248 was 15.09% for SnO<sub>2</sub>/CdO/Si DLSC as measured while 12.28% for original c-Si solar cells. In  
249 addition, the recombination of photogenerated carriers were greatly restrained, resulting in a high  
250 minority carrier lifetime value. It is believed that by using band-gap alignment engineering,  
251 crystalline silicon solar cells still have deeper potential for further exploration.

252 **Acknowledgments:** This study is supported by the Key Project of Excellent Youth Talent Support Plan of  
253 Anhui Province (gxyqZD2016540), Natural Science Foundation of Education Department of Anhui Province  
254 (KJ2018A0834), Natural Science Foundation of Education Department of Anhui Province (KJ2017ZD49), Talent  
255 Project of the College (ZD2017004) and PCSIRT (IRT\_16R49).

256 **Author Contributions:** Lingling Zhou performed the experiments, analyzed the data and wrote the paper;  
257 Lufei Xiao analyzed the data; Hai Yang performed the experiments, analyzed the data and revised the paper;  
258 Jie Liu conceived, designed the experiments and revised the paper; Xibin Yu conceived and designed the  
259 experiments.

260 **Conflicts of Interest:** The authors declare no conflicts of interest.

#### 261 References

- 262 1. Cotal, H.; Fetzer, C.; Boisvert, J.; Kinsey, G.; King, R.; Hebert, P.; Yoon, H.; Karam, N. III–V multijunction  
263 solar cells for concentrating photovoltaics. *Energy Environ. Sci.* 2009, **2**, 174-192, DOI: 10.1039/B809257E.
- 264 2. Bertness, K. A.; Kurtz, S. R.; Friedman, D. J.; Kibbler, A. E.; Kramer, C.; Olson, J. M. 29.5%-efficient  
265 GaInP/GaAs tandem solar cells. *Appl. Phys. Lett.* 1994, **65**, 989-991, DOI: 10.1063/1.112171.
- 266 3. Yamaguchi, M.; Takamoto, T.; Araki, K.; Ekins-Daukes, N. Multi-junction III–V solar cells: current status  
267 and future potential. *Solar Energy*. 2005, **79**, 78-85, DOI: 10.1016/j.solener.2004.09.018.
- 268 4. Siddiki, M. K.; Li, J.; Galipeau, D.; Qiao, Q. A review of polymer multijunction solar cells. *Energy Environ.*  
269 *Sci.* 2010, **3**, 867-883, DOI: 10.1039/b926255p.
- 270 5. Priolo, F.; Gregorkiewicz, T.; Galli, M.; Krauss, T. F.; *Nature Nanotech.* 2014, **9**, 19-32, DOI:  
271 10.1038/nnano.2013.271.

- 272 6. Tisdale, W. A.; Williams, K. J.; Timp, B. A.; Norris, D. J.; Aydil, E. S.; Zhu X. Y. Hot-electron transfer from  
273 semiconductor nanocrystals. *Science* 2010, **328**, 1543-1547, DOI: 10.1126/science.1185509.
- 274 7. Green, M. A. Solar cells: Operating Principles, Technology and System Applications. The University of  
275 New South Wales, Sydney, Australia, 1998.
- 276 8. Wang, X.; Peng, K. Q.; Pan, X. J.; Chen, X.; Yang, Y.; Li, L.; Meng, X. M.; Zhang, W. J.; Lee, S. T.  
277 High-performance silicon nanowire array photoelectrochemical solar cells through surface passivation  
278 and modification. *Angew. Chem., Int. Ed.* 2011, **50**, 9861-9865, DOI: 10.1002/anie.201104102.
- 279 9. Garnett, E.; Yang, P. Light trapping in silicon nanowire solar cells. *Nano Lett.* 2010, **10**, 1082-1087, DOI:  
280 10.1021/nl100161z.
- 281 10. Peng, K. Q.; Lee, S. T. Silicon nanowires for photovoltaic solar energy conversion. *Adv. Mater.* 2011, **23**,  
282 198-215, DOI: 10.1002/adma.201002410.
- 283 11. Pudasaini, P. R.; Ruiz-Zepeda, F.; Sharma, M.; Elam, D.; Ponce, A.; Ayon, A. A. High efficiency hybrid  
284 silicon nanopillar-polymer solar cells. *ACS Appl. Mater. Interfaces* 2013, **5**, 9620-9627, DOI:  
285 10.1021/am402598j.
- 286 12. Xia, Y. S.; Pu, X. X.; Liu, J.; Liang, J.; Liu, P. J.; Li, X. Q.; Yu, X. B. CuO nanoleaves enhance the c-Si solar cell  
287 efficiency. *J. Mater. Chem. A* 2014, **2**, 6796-6800, DOI: 10.1039/C4TA00097H.
- 288 13. Ferry, V. E.; Verschuuren, M. A.; Lare, M. C.; Schropp, R. E. I.; Atwater, H. A.; Polman, A. Optimized  
289 spatial correlations for broadband light trapping nanopatterns in high efficiency ultrathin film a-Si:H solar  
290 cells. *Nano Lett.* 2011, **11**, 4239-4245, DOI: 10.1021/nl202226r.
- 291 14. Wang, K. X.; Yu, Z.; Liu, V.; Cui, Y.; Fan, S. Absorption enhancement in ultrathin crystalline silicon solar cells  
292 with antireflection and light-trapping nanocone gratings. *Nano Lett.* 2012, **12**, 1616-1619, DOI:  
293 10.1021/nl204550q.
- 294 15. Yu, R.; Lin, Q.; Leung, S.-F.; Fan, Z. Nanomaterials and nanostructures for efficient light absorption and  
295 photovoltaics. *Nano Energy*. 2012, **1**, 57-72, DOI: 10.1016/j.nanoen.2011.10.002.
- 296 16. Eisler, C. N.; Abrams, Z. R.; Sheldon, M. T.; Zhang, X.; Atwater, H. A. Multijunction solar cell efficiencies:  
297 effect of spectral window, optical environment and radiative coupling. *Energy Environ. Sci.* 2014, **7**,  
298 3600-3605, DOI: 10.1039/C4EE01060D.
- 299 17. Ameri, T.; Dennler, G.; Lungenschmied, C.; Brabec, C. J. Organic tandem solar cells: A review. *Energy*  
300 *Environ. Sci.* 2009, **2**, 347-363, DOI: 10.1039/B817952B.
- 301 18. Dou, L.; You, J.; Yang, J.; Chen, C.-C.; He, Y.; Murase, S.; Moriarty, T.; Emery, K.; Li, G.; Yang, Y. Tandem  
302 polymer solar cells featuring a spectrally matched low-bandgap polymer. *Nature Photon.* 2012, **6**, 180-185,  
303 DOI: 10.1038/nphoton.2011.356.
- 304 19. Gilot, J.; Wienk, M. M.; Janssen, René A. J. Double and triple junction polymer solar cells processed from  
305 solution. *Appl. Phys. Lett.* 2007, **90**, 143512, DOI: 10.1063/1.2719668.
- 306 20. Dennler, G.; Scharber, M. C.; Brabec, C. J. Polymer-fullerene bulk-heterojunction solar cells. *Adv. Mater.*  
307 2009, **21**, 1323-1338, DOI: 10.1002/adma.200801283.
- 308 21. Chuang, C.-H. M.; Brown, P. R.; Bulović, V.; Bawendi, M. G. Improved performance and stability in  
309 quantum dot solar cells through band alignment engineering. *Nat. Mater.* 2014, **13**, 796-801, DOI:  
310 10.1038/nmat3984.



- 311 22. Saha, B.; Thapa, R.; Chattopadhyay, K. K. Bandgap widening in highly conducting CdO thin film by Ti  
312 incorporation through radio frequency magnetron sputtering technique. *Solid State Commun.* 2008, **145**,  
313 33-37, DOI: 10.1016/j.ssc.2007.10.001.
- 314 23. Ueda, N.; Maeda, H.; Hosono, H.; Kawazoe, H. Band-gap widening of CdO thin films. *J. Appl. Phys.* 1998,  
315 **84**, 6174-6177, DOI: 10.1063/1.368933.
- 316 24. Wang, H. P.; Lien, D. H.; Tsai, M. L.; Lin, C. A.; Chang, H. C.; Lai, K. Y.; He, J. H. Photon management in  
317 nanostructured solar cells. *J. Mater. Chem. C* 2014, **2**, 3144-3171, DOI: 10.1039/C3TC32067G.
- 318 25. Liu, X. G.; Coxon, P. R.; Peters, M.; Hoex, B.; Cole, J. M.; Fray, D. J. Black silicon: fabrication methods,  
319 properties and solar energy applications. *Energy Environ. Sci.* 2014, **7**, 3223-3263, DOI: 10.1039/c4ee01152j.
- 320 26. Chen, G. Y.; Seo, J. W.; Yang, C. H.; Prasad, P. N. Nanochemistry and nanomaterials for photovoltaics.  
321 *Chem. Soc. Rev.* 2013, **42**, 8304-8338, DOI: 10.1039/C3CS60054H.
- 322 27. Zhuang, X. J.; Ning, C. Z.; Pan, A. Composition and bandgap-graded semiconductor alloy nanowires. *Adv.*  
323 *Mater.* 2012, **24**, 13-33, DOI: 10.1002/adma.201103191.
- 324 28. Xie, C.; Zhang, X.; Ruan, K.; Shao, Z.; Dhaliwal, S. S.; Wang, L.; Zhang, Q.; Zhang, X.; Jie, J. High-efficiency,  
325 air stable graphene/Si micro-hole array Schottky junction solar cells. *J. Mater. Chem. A.* 2013, **1**, 15348-15354,  
326 DOI: 10.1039/C3TA13750C.
- 327 29. Baek, S. H.; Kim, S.-B.; Shin, J. K.; Kim, J. H. Preparation of hybrid silicon wire and planar solar cells  
328 having ZnO antireflection coating by all-solution processes. *Sol. Energy Mater. Sol. Cells.* 2012, **96**,  
329 251-256, DOI: 10.1016/j.solmat.2011.10.007.
- 330 30. Polman, A.; Atwater, H. A. Photonic design principles for ultrahigh-efficiency photovoltaics. *Nat. Mater.*  
331 2012, **11**, 174-177, DOI: 10.1038/nmat3263.
- 332 31. Sinton, R. A.; Cuevas, A. Contactless determination of current-voltage characteristics and minority-carrier  
333 lifetimes in semiconductors from quasi-steady-state photoconductance data. *Appl. Phys. Lett.* 1996, **69**,  
334 2510-2512, DOI: 10.1063/1.117723.
- 335 32. Wang, H. P.; Lin, T. Y.; Tsai, M. L.; Tu, W. C.; Huang, M. Y.; Liu, C. W.; Chueh, Y. L.; He, J. H. Toward  
336 efficient and omnidirectional n-type Si solar cells: concurrent improvement in optical and electrical  
337 characteristics by employing microscale hierarchical structures. *ACS Nano.* 2014, **8**, 2959-2969, DOI:  
338 10.1021/nn500257g.
- 339 33. Yang, W. L.; Liu, Y.; Hu, Y.; Zhou, M. J.; Qian, H. S. Microwave-assisted synthesis of porous CdO-CdS  
340 core-shell nanoboxes with enhanced visible-light-driven photocatalytic reduction of Cr(VI). *J. Mater. Chem.*  
341 2012, **22**, 13895-13898, DOI: 10.1039/C2JM33010E.
- 342 34. Li, W.; Li, M. Y.; Xie, S. L.; Zhai, T.; Yu, M. H.; Liang, C. L.; Ouyang, X. W.; Lu, X. H.; Li, H. H.; Tong, Y. X.  
343 Improving the photoelectrochemical and photocatalytic performance of CdO nanorods with CdS  
344 decoration. *CrystEngComm.* 2013, **15**, 4212-4216, DOI: 10.1039/C3CE40092A.